

# Fabrication of porous Ag by dealloying of Ag-Zn alloys in H<sub>2</sub>SO<sub>4</sub> solution

Z. Q. Li · B. Q. Li · Z. X. Qin · X. Lu

Received: 5 April 2010/Accepted: 24 June 2010/Published online: 7 July 2010  
© Springer Science+Business Media, LLC 2010

**Abstract** In the present work, the fabrication of porous silver through the dealloying of Ag<sub>24.3</sub>Zn<sub>75.7</sub>, Ag<sub>33.4</sub>Zn<sub>66.6</sub>, and Ag<sub>57.6</sub>Zn<sub>42.4</sub> alloys in dilute H<sub>2</sub>SO<sub>4</sub> solution is reported. Different length scales and distribution could be achieved through varying the alloy's composition and concentration of H<sub>2</sub>SO<sub>4</sub> solution. Multi-porosity distribution of Ag<sub>33.4</sub>Zn<sub>66.6</sub> alloy also indicates the possibility to tailor the microfilter's structure by using common microstructure controlling method in materials science.

## Introduction

Due to the potential applications in molecular adsorptions, ion exchange, medical materials, and heterogeneous catalysis, fabrication of porous Ag and Ag nanoparticles were actively investigated in recent years [1–8]. The most works on porous Ag formation is based on employing colloidal crystal template [9]. For example, Mann and coworkers [10] describe a self-supporting macroporous framework of Ag, Au, and copper oxide by employing dextran as the template. The cellulose fiber as scaffolds has been used to fabricate porous Ag nanostructures [11]. Poly(ethyleneimine) hydrogel has also been used as a soft template to make macroporous silver frameworks [12]. Porous Ag monoliths can also be prepared in a one-pot reaction [13] using silica hydrogel as the template. A method to synthesize porous silver monoliths using a simple surfactant cum reductant, Triton X-114, as the sacrificial template, is recently reported [14]. And the

porous Ag can also be achieved by the method of electrochemical deposition, the porosity is 95–98% and surface area is more than 1.0 m<sup>2</sup>/g [15, 16].

Since the pioneer works by Sieradsky and Erlebacher [17, 18], dealloying (selective dissolution) is demonstrating its potential to fabricate the nanoporous metals. As it can transform initially dense alloys into materials with a uniform, open porosity, with ligament widths and spacings tunable between just a few nanometers to many hundreds of nanometers, and usually employing only the simplest electrochemical processing in any system where a large electrochemical potential difference exists between the alloying elements. Yeh et al. [19] reported formation of porous silver by electrochemical alloying/dealloying in a water-insensitive zinc chloride-1-ethyl-3-methyl imidazolium chloride ionic liquid. Jia et al. [20] fabricated nanoporous metals (Cu, Ag, Au) by electrodeposition of Zn on the metal surfaces, thermal alloying, and chemical dealloying of Zn. In the present article, the dealloying of three Ag-Zn alloys in H<sub>2</sub>SO<sub>4</sub> solution and relationship between the porous feature and alloy composition will be reported.

## Experimental

The alloys were prepared by induction melting from zinc granules (99.97%) and silver plates (99.99%) under Ar protection of 0.05 MPa after vacuuming to 5 × 10<sup>-3</sup> Pa. The alloys compositions (at.%) measured by Oxford INCA energy dispersive X-ray analysis (EDX) are Ag<sub>24.3</sub>Zn<sub>75.7</sub>, Ag<sub>33.4</sub>Zn<sub>66.6</sub>, and Ag<sub>57.6</sub>Zn<sub>42.4</sub>, respectively. Ag<sub>24.3</sub>Zn<sub>75.7</sub> and Ag<sub>33.4</sub>Zn<sub>66.6</sub> were annealed at 550 °C for a week and then quenched into cold water; Ag<sub>57.6</sub>Zn<sub>42.4</sub> was annealed at 650 °C for the same treatment. The anodic polarization curves of alloys were measured by LK98 II potentiostat in

Z. Q. Li (✉) · B. Q. Li · Z. X. Qin · X. Lu  
Liaoning Key Materials Laboratory for Railway, Dalian Jiaotong  
University, Dalian 116028, People's Republic of China  
e-mail: lizhiqiang201@126.com

0.1 M and 0.01 M H<sub>2</sub>SO<sub>4</sub> aqueous solution, respectively. The electrodes consisted of a Pt counter electrode, a saturated calomel reference electrode (SCE), and the alloy tested as the working electrode. Rigaku D/max-ULTMA<sup>+</sup> X-ray diffractometer employing CuK $\alpha$  radiation determined the crystal structure. The morphology of the surface was examined with scanning electron microscope (JSM-6360LV).

## Results and discussion

### The crystal structure of Ag-Zn alloys

The crystal structures of three alloys were checked by X-ray diffraction, as shown in Fig. 1. The results show that hexagonal  $\varepsilon$  phase exists in Ag<sub>24.3</sub>Zn<sub>75.7</sub> alloy; body-centered cubic  $\beta$  phase in Ag<sub>57.6</sub>Zn<sub>42.4</sub> alloy; hexagonal  $\varepsilon$  and body-centered cubic  $\gamma$  phases in Ag<sub>33.4</sub>Zn<sub>66.6</sub>, which are in good agreement with the equilibrium Ag-Zn phase diagram [21].

### The anodic polarization behavior of Ag-Zn alloys

Figure 2 shows the anodic polarization behavior of Ag-Zn alloys in 0.01 M and 0.1 M H<sub>2</sub>SO<sub>4</sub> solution, for clarity of presentation, a small percentage of the cathodic branch was included. Regardless of the big diversity of alloy's composition, their anodic polarization behaviors are roughly identical. The profile of curves is quite similar to that of Au-Ag alloys in 1 M AgClO<sub>4</sub> + 1 M HClO<sub>4</sub> solution [22], which foreshows the possibility to undergo a dealloying. With increasing concentration of H<sub>2</sub>SO<sub>4</sub> (comparing (a) and (b) of Fig. 2), the corrosion current density increases and the self-corrosion potential decreases. The inset in

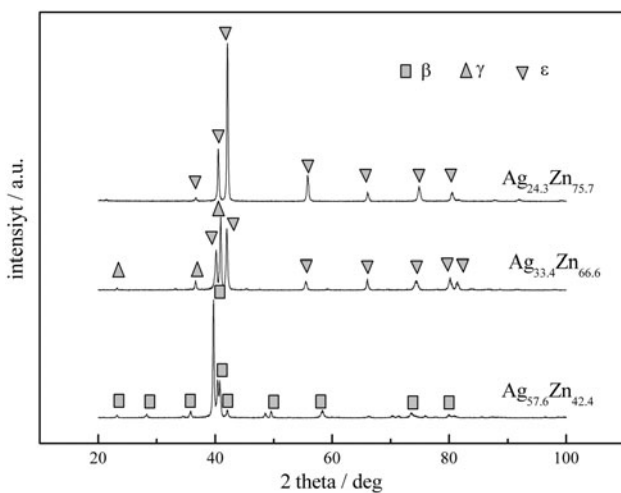


**Fig. 1** X-ray diffraction patterns of Ag-Zn alloys

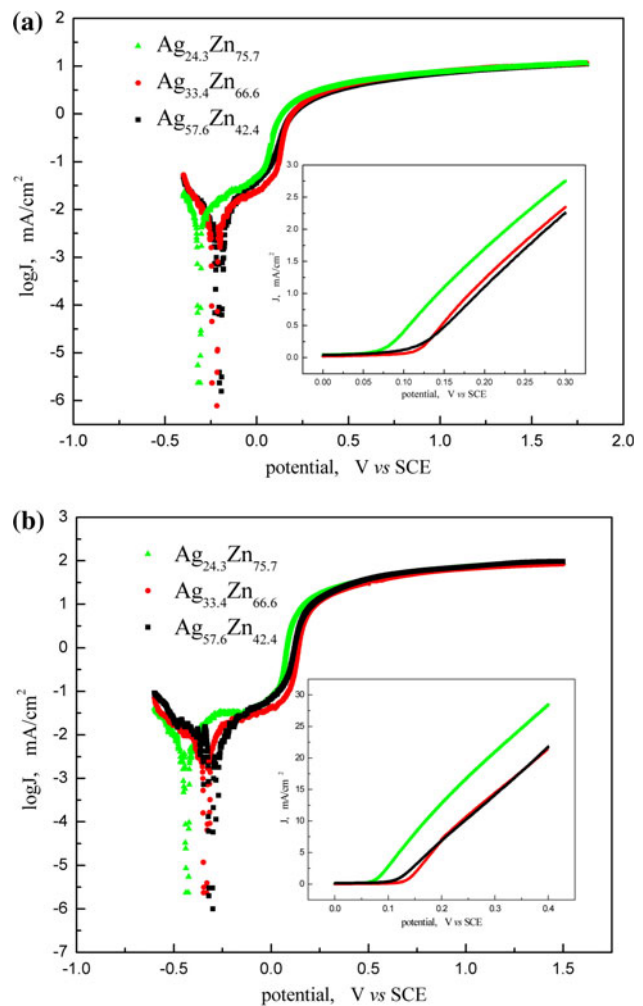


**Fig. 2** Anodic polarization curves for Ag-Zn alloys in 0.01 M H<sub>2</sub>SO<sub>4</sub> (a) and 0.1 M H<sub>2</sub>SO<sub>4</sub> (b), scan rate 1 mV/s. Inset shows current density on a linear scale near the critical potential

Fig. 2 shows the same data on a linear scale over a narrow range of potential. The rapid increase rate in the dissolution observed in the inset of Fig. 2 at a potential of about 0.1 V (SCE) is indicative of the onset of dealloying and is referred to in the literature as the dealloying critical potential. Table 1 lists the self-corrosion potential and critical potentials of the alloys in 0.01 M and 0.1 M H<sub>2</sub>SO<sub>4</sub> solution, where with decreasing Ag content and increasing

**Table 1** The self-corrosion potential and critical potential (V, SCE) of Ag-Zn alloys

Alloy	0.01 M H <sub>2</sub> SO <sub>4</sub>		0.1 M H <sub>2</sub> SO <sub>4</sub>	
	V <sub>self</sub>	V <sub>crit</sub>	V <sub>self</sub>	V <sub>crit</sub>
Ag <sub>24.3</sub> Zn <sub>75.7</sub>	-0.32	0.14	-0.42	0.08
Ag <sub>33.4</sub> Zn <sub>66.6</sub>	-0.21	0.20	-0.35	0.14
Ag <sub>57.6</sub> Zn <sub>42.4</sub>	-0.19	0.19	-0.30	0.12

the concentration of  $H_2SO_4$  solution from 0.01 to 0.1 M, both the self-corrosion potential and critical potential decreases, which means a stronger inclination to dealloying.

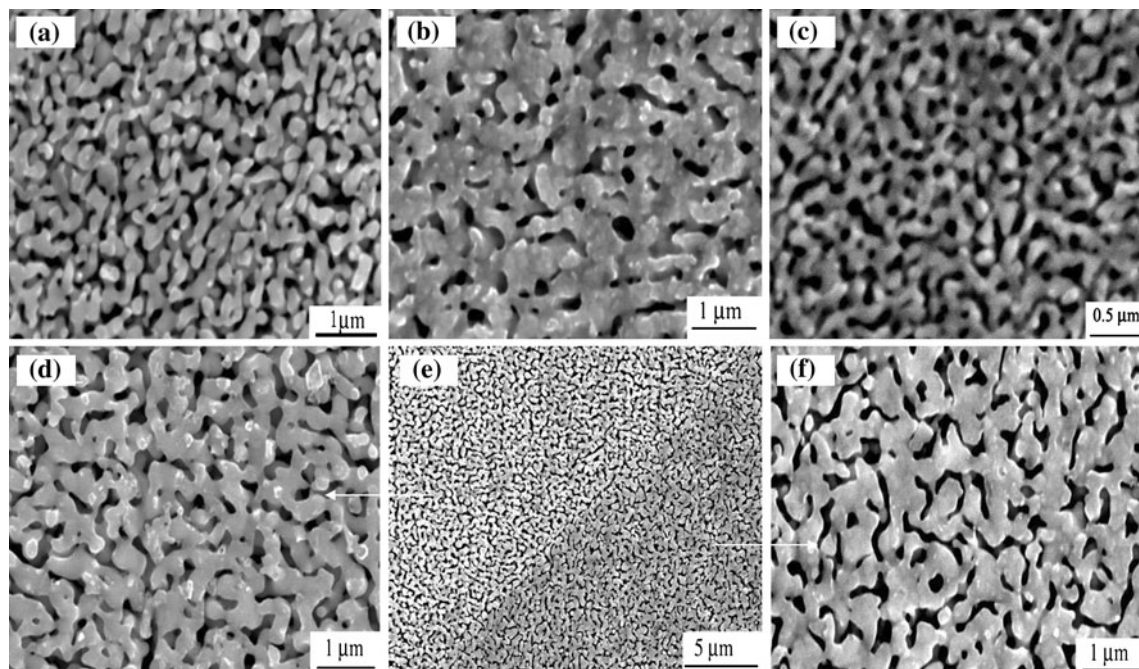
### Morphology of porous Ag by dealloying of Ag–Zn

According to the anodic polarization behavior of Ag–Zn alloys, we select 0.6 V (SCE) and 1.5 V (SCE) as the dealloying potential, which is higher than the critical potential. Figure 3 presents the results of dealloying for three Ag–Zn alloys in  $H_2SO_4$  solution. Figure 3a shows typical uniform interconnected pore characteristic with average pore size of about 140 nm from original  $\epsilon$  phase, i.e.,  $Ag_{24.3}Zn_{75.7}$ , which is similar to that of Jia et al. [20]. EDX measurement verifies that Zn has been completely dissolved, which suggests that the product of dealloying is porous Ag. The cracks occurred during dealloying, which has been reported in Ag–Au system [23], are also visible in the present alloy.

In Fig. 3b, the SEM image of  $Ag_{57.6}Zn_{42.4}$  shows uniform pore characteristic too, however, with less pores (average size 190 nm) and bigger ligaments. The EDX measurement detected only traces of Ag existing, which implies that the dealloying of  $\beta$  phase occurred too. Dursun et al. [24] have shown that the size scale of porosity produced during the dealloying of  $Ag_{0.65}Au_{0.35}$  in 0.1 M  $HClO_4$  electrolytes was found to increase with the addition of halides. In the present investigation, the pore size could

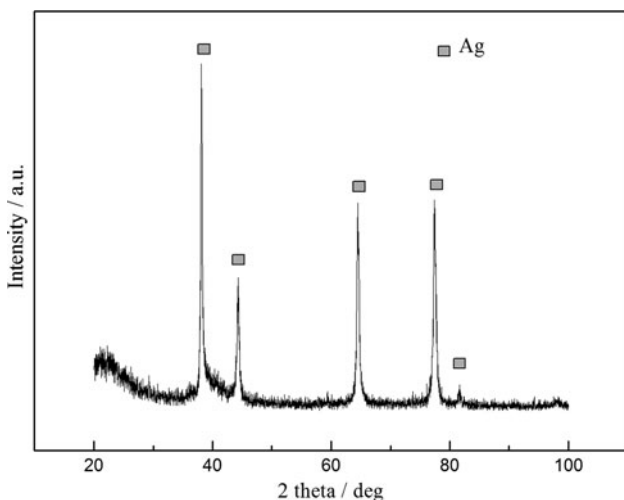
also be modified by varying the concentration of  $H_2SO_4$  or the potential. Figure 3c shows an example of  $Ag_{24.3}Zn_{75.7}$  dealloyed at 1.5 V (SCE) for 90 min in 0.01 M  $H_2SO_4$  solution, showing an average pore size of 85 nm, about a half of that dealloyed at 0.6 V (SCE) for 30 min in 0.1 M  $H_2SO_4$  solution.

Figure 3e presents the result of  $Ag_{33.4}Zn_{66.6}$  after the same dealloying treatment. There are two regions, which show different pore feature due to original binary phases of  $\epsilon + \gamma$ : the image on top-left of Fig. 3e is amplified as Fig. 3d and the image on bottom-right as Fig. 3f at the same amplification. The surface morphology in Fig. 3d is similar to Fig. 3a, except with fewer pores. The bigger ligaments in Fig. 3f could be found comparing with that in Fig. 3d, which means that fewer pores exist in Fig. 3f. The average pore size is about 176 and 180 nm in Fig. 3d and f, respectively. As have been shown above,  $Ag_{33.4}Zn_{66.6}$  alloy consists of  $\epsilon$  and  $\gamma$  phase. Since the alloy was annealed at 550 °C and then quenched into water, the Zn content in  $\epsilon$  and  $\gamma$  is supposed to be about 67 and 64 at.%, respectively. Therefore, the top-left region in Fig. 3e should be from  $\epsilon$  and the bottom-right from  $\gamma$ . Irrespective of the difference of morphology, the ligaments in both regions are made of pure Ag, as proved by EDX measurements. In addition, there are continuous pores exist along the phase boundary, which implies the preference dissolution here [23] and also the possible weakness upon tensile stress. The distinct boundary itself implies that little long-distance surface



**Fig. 3** SEM images of **a**  $Ag_{24.3}Zn_{75.7}$ , 0.6 V for 30 min in 0.1 M  $H_2SO_4$ ; **b**  $Ag_{57.6}Zn_{42.4}$ , 0.6 V for 30 min in 0.1 M  $H_2SO_4$ ; **c**  $Ag_{24.3}Zn_{75.7}$ , 1.5 V for 90 min in 0.01 M  $H_2SO_4$ ; **e**  $Ag_{33.4}Zn_{66.6}$ ,

0.6 V for 30 min in 0.1 M  $H_2SO_4$ ; **d** and **f** are the amplification of top-left and bottom-right parts of (e), respectively



**Fig. 4** X-ray diffraction pattern of  $\text{Ag}_{33.4}\text{Zn}_{66.6}$  after dealloying at 0.6 V for 30 min in 0.1 M  $\text{H}_2\text{SO}_4$ , showing the existence of single Ag

diffusion of Ag atoms occurs across boundary during dealloying.

Erlebacher et al. [18] have revealed the following qualitative picture of porosity formation on the model of Au–Ag system. The process is modeled in terms of diffusive redistribution of components (gold and vacancies) on a crystal lattice (Au–Ag is a continuous solid solution). Although new ligaments are continuously formed by bifurcation of pores that have sufficiently penetrated into the bulk, the mechanism does not require either nucleation of new crystallites nor the formation or removal of lattice sites [25]. As far as the Ag–Zn system is concerned, the crystal structures of hexagonal  $\epsilon$  phase, body-centered cubic  $\gamma$ , and body-centered cubic  $\beta$  phase are different from face-centered cubic Ag (Fig. 4 showing an X-ray diffraction pattern of porous Ag after dealloying  $\text{Ag}_{33.4}\text{Zn}_{66.6}$  at 0.6 V for 30 min in 0.1 M  $\text{H}_2\text{SO}_4$ ). As the Ag adatoms diffuse about and start to agglomerate into islands, nucleation of new FCC crystallites occurs, which means reconstruction of Ag atoms from complicate-structured intermetallic compound to simple FCC Ag during dealloying. For this reason, the orientation relation of crystals between the parent phases and FCC Ag should be further studied for clarifying the atomic mechanism of dealloying in Ag–Zn system.

## Conclusions

It was shown that different length scales and distribution which exhibits an unusual three-dimensional pattern-forming instability could be achieved through varying the starting alloy's composition and concentration of  $\text{H}_2\text{SO}_4$

solution or varying the electrochemical potential driving dissolution. The ease of production of porous silver may make this method of processing attractive for applications such as high surface area biomedical electrodes, microfilters, or as catalyst materials. Multi-porosity distribution of  $\text{Ag}_{33.4}\text{Zn}_{66.6}$  alloy also indicates the possibility to tailor the microfilter's structure by using common microstructure controlling method in materials science.

**Acknowledgements** The project has been financially supported by Higher Education Doctoral Fund of China (20080150002), and Ministry of Education, Liaoning Province's Government, China (RC-04-15).

## References

- Yaghi OM, Li G, Li H (1995) Nature 378:703
- Yaghi OM, Li H, Am J (1995) Chem Soc 117:10401
- Alammar T, Mudring AV (2009) J Mater Sci 44:3218. doi: [10.1007/s10853-009-3429-4](https://doi.org/10.1007/s10853-009-3429-4)
- Bera T, Ramachandrarao P (2009) J Mater Sci 44:2264. doi: [10.1007/s10853-008-2861-1](https://doi.org/10.1007/s10853-008-2861-1)
- Uznanski P, Bryszewska E (2010) J Mater Sci 45:1547. doi: [10.1007/s10853-009-4122-3](https://doi.org/10.1007/s10853-009-4122-3)
- Ilic V, Saponjic Z, Vodnik V et al (2009) J Mater Sci 44:3983. doi: [10.1007/s10853-009-3547-z](https://doi.org/10.1007/s10853-009-3547-z)
- Govindaraju K, Basha SK, Kumar VG et al (2008) J Mater Sci 43:5115. doi: [10.1007/s10853-008-2745-4](https://doi.org/10.1007/s10853-008-2745-4)
- Huang YP, Yang Y, Chen Z et al (2008) J Mater Sci 43:5390. doi: [10.1007/s10853-008-2793-9](https://doi.org/10.1007/s10853-008-2793-9)
- Velev OD, Tessier PM, Lenhoff AM, Kaler EW (1999) Nature 401:548
- Walsh D, Arcelli L, Ikoma T, Tanaka J, Mann S (2003) Nature Mater 2:386
- He J, Kunitake T, Watanabe T (2005) Chem Commun 795
- Jin RH, Yuan JJ (2005) J Mater Chem 15:4513
- Sisk CN, Gill SK, Weeks LJH (2006) Chem Lett 35:814
- Khan F, Eswaramoorthy M, Rao CNR (2007) Solid State Sci 9:27
- Luo YH, Guo L, Jiang HY (2005) Nonferrous Met (Extr Metall) 5:43
- Li BS, Niu YS (2000) Petrochem Technol 29:910
- Li R, Sieradzki K (1992) Phys Rev Lett 68:1168
- Erlebacher J, Aziz MJ, Karma A, Dimitrov N, Sieradzki K (2001) Nature (London) 410:450
- Yeh FH, Tai CC, Huang JF, Sun IW (2006) J Phys Chem B 110:5215
- Jia FL, Yu CF, Deng KJ, Zhang LZ (2007) J Phys Chem C 111:8424
- Massalski TB (1986) Binary alloy phase diagram. American Society for Metals, Metals Park, OH
- Sieradzki K, Dimitrov N, Movrin D, McCall C, Vasiljevic N, Erlebacher J (2002) J Electrochem Soc 149:B370
- Lu X, Balk TJ, Spolenak R, Arzt E (2007) Thin Solid Films 515:7122
- Dursun A, Pugh DV, Corcoran SG (2003) J Electrochem Soc 150:B355
- Parida S, Kramer D, Volkert CA, Roesner H, Erlebacher J, Weissmuller J (2006) Phys Rev Lett 97:035504